Electronic Supplementary Material (ESI) for Energy & Environmental Science

Supporting Information

Sub 150 °C Processed Meso-superstructured Perovskite Solar Cells with Enhanced Efficiency

Konrad Wojciechowski, Michael Saliba, Tomas Leijtens, Antonio Abate and Henry J. Snaith*

* Department of Physics, University of Oxford, Clarendon Laboratory, Parks Road, Oxford OX1 3PU, UK. E-mail: h.snaith1@physics.ox.ac.uk

1. SEM images of TiO_2 compact layers

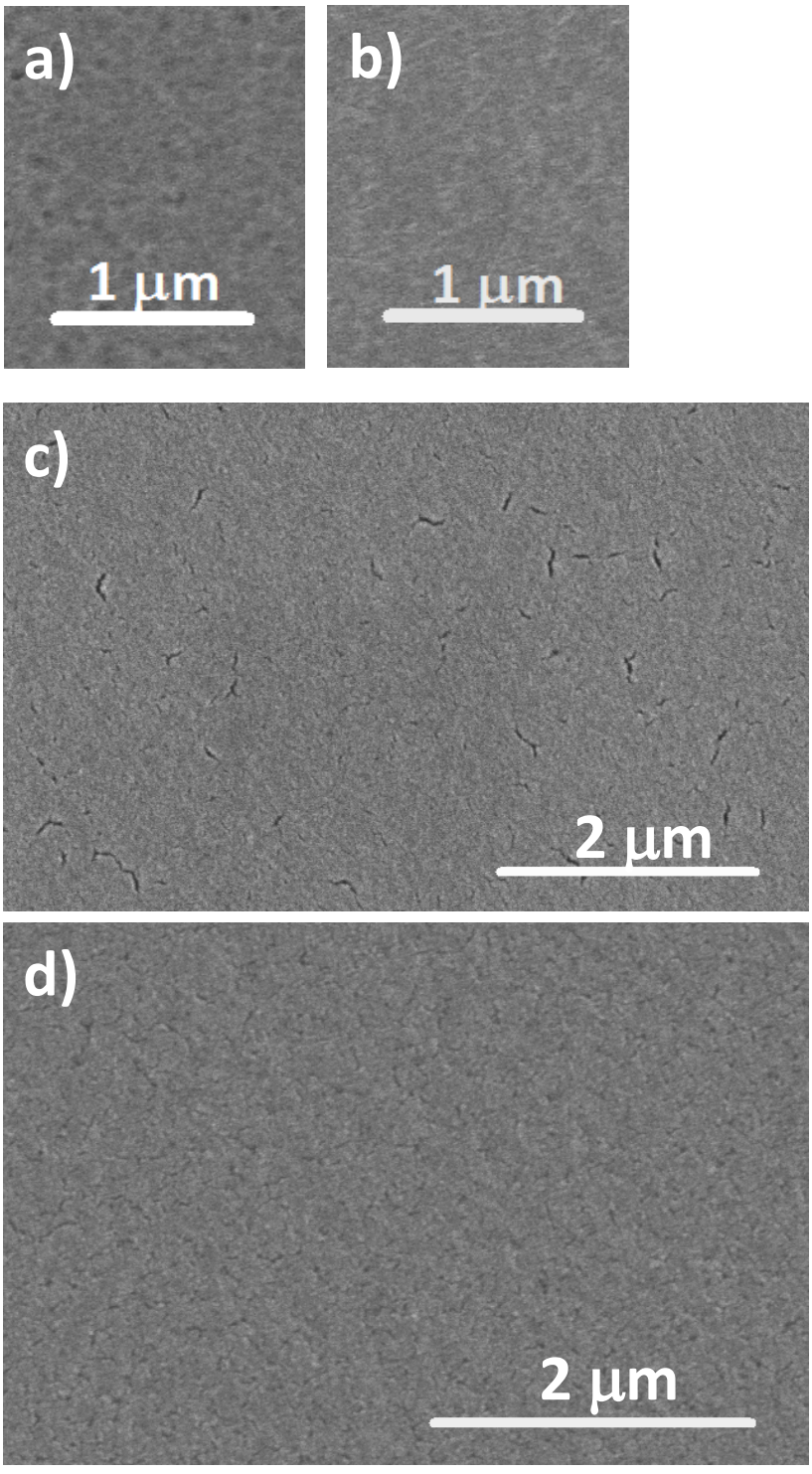

Figure S1. SEM image of the top surface of TiO_x (a); ht-TiO_2 (b); lt-TiO_2-0% TiAcAc (c); lt-TiO_2-20% TiAcAc (d).

2. Optimization of TiO_2 nanoparticles formulation

2.1. TiAcAc concentration dependence

Devices with the additive show clear improvement in J_{sc}, which could be attributed to a better interconnection between particles resulting in an improved charge transport properties. With increased TiAcAc concentration, the amount of amorphous TiO_x in the film increases resulting in a worse device performance, mainly due to a drop of V_{oc} and J_{sc}. 10% and 20% TiAcAc works the best, the former one benefits in slightly higher J_{sc} and V_{oc} compared to the latter, but loses in lower fill factor.

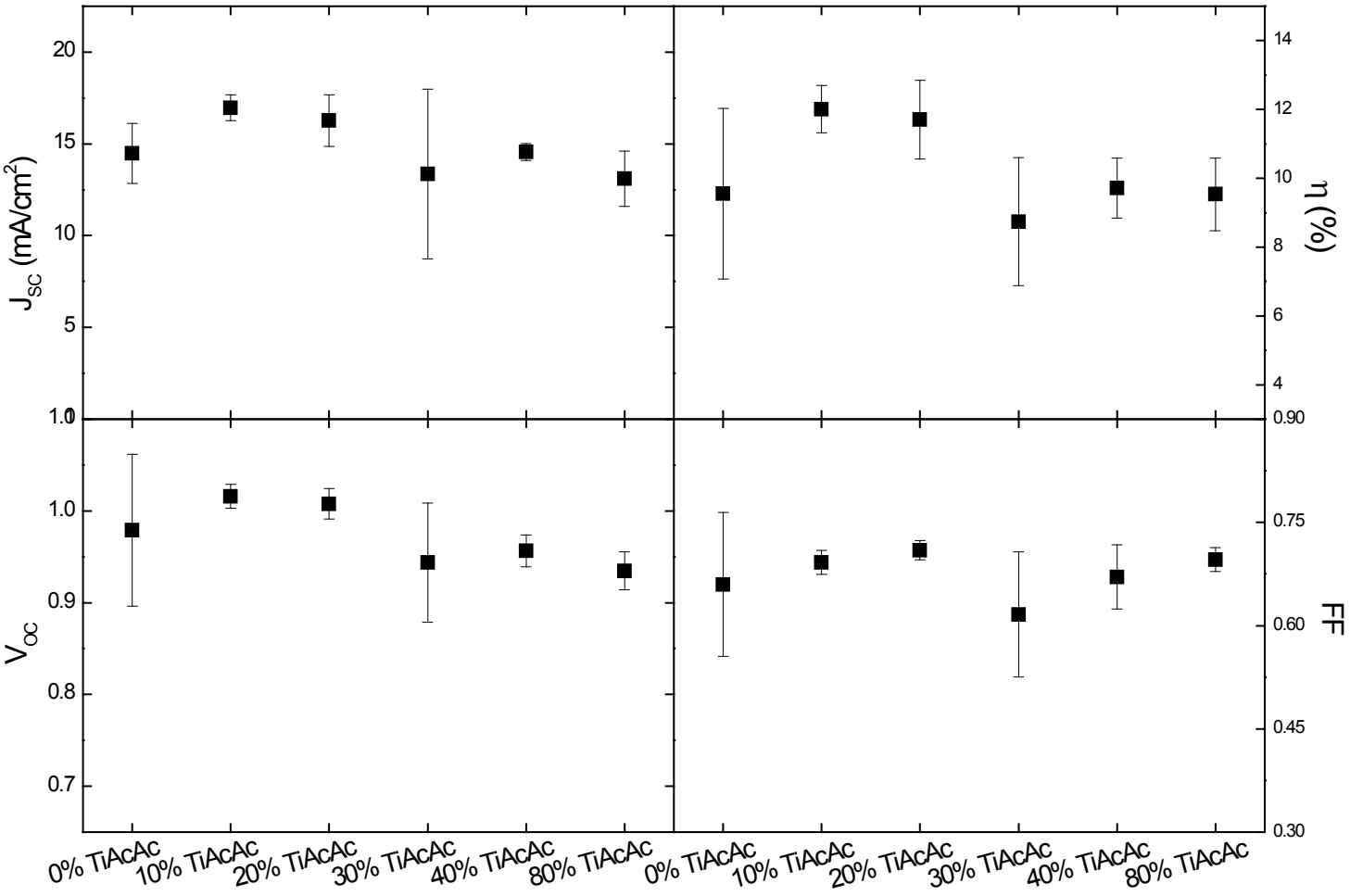

Figure S2. Photovoltaic parameters (short-circuit current density - J_{SC}, solar cell efficiency – η, open-circuit voltage – V_{OC} and fill factor – FF) extracted from current-voltage measurements of devices with varying concentration of TiAcAc additive in a compact layer.

2.2. Compact layer thickness dependence.

We varied the thickness of the compact layer by changing the concentration of TiO_2 nanoparticles from 3.54 weigth% to 0.24 weight%. On a flat glass substrate, formulations resulted in thicknesses from 110 nm to <10 nm The optimum formulation is between 1.2% and 1.8% TiO_2. Devices with thinner compact layers are mainly affected by a drop of fill factor, and J_{sc}. Due to the roughness of FTO (see Figure 2b), diluted formulations are less likely to completely cover the surface of the electrode. Uninhibited recombination by electron leakage from FTO to perovskite can cause the drop of the performance in those devices. The more concentrated TiO_2 formulation (>3%), yielding over 110 nm thick film on a flat glass, is mainly affected by the drop in V_{oc}. In thicker TiO_2 film there might be more unfilled sub-band gap trap states due to lower charge density (charges dissipate over the bigger space), which could result in a lower quasi Fermi-level for electrons and drop of V_{oc}.

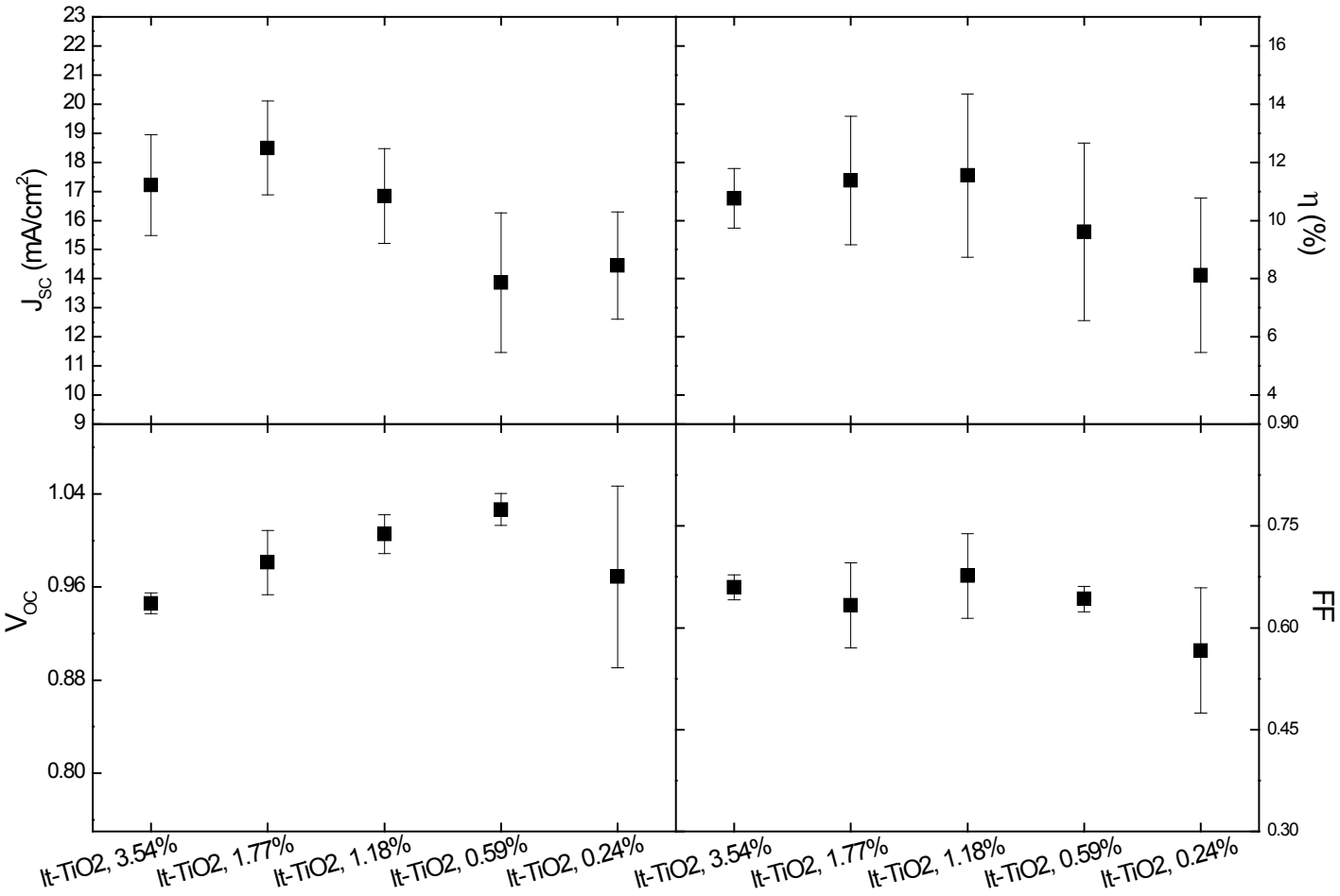

Figure S3. Photovoltaic parameters extracted from current-voltage measurements of the devices with varying low temperature TiO_2 (lt-TiO_2) compact layer thickness.

2.3. Reoptimised concentration of perovskite precursor solution.

We fabricated a batch of devices (12) for the optimised lt-TiO_2 and ht-TiO_2 with higher perovskite concentration resulting in higher J_{sc} and overall photovoltaic performance.

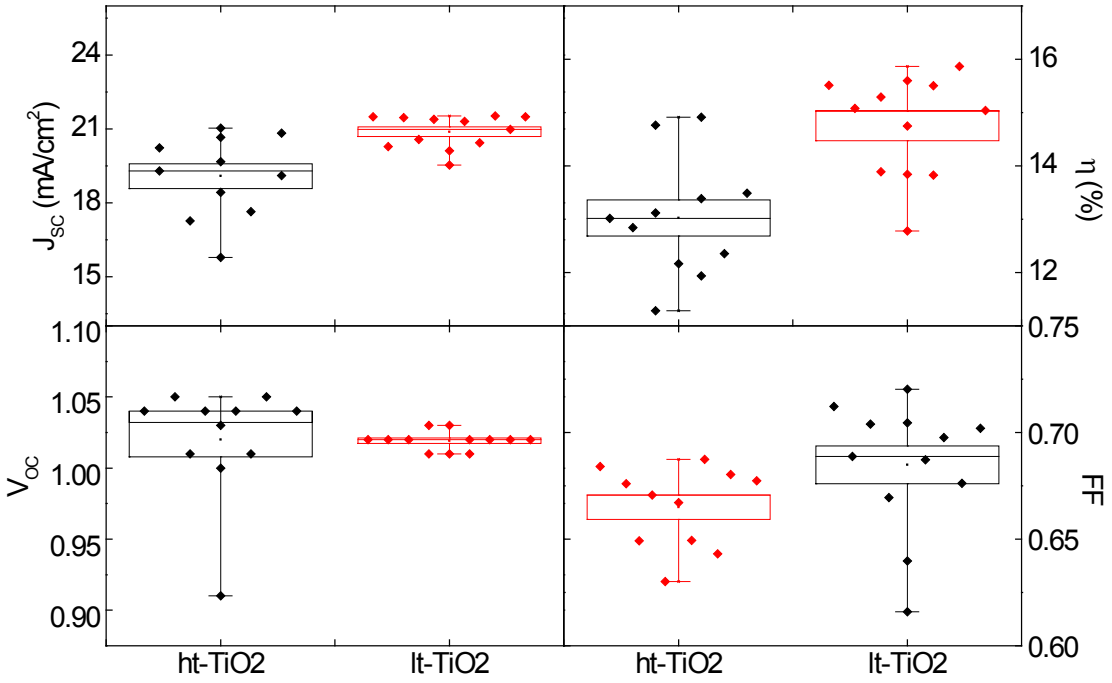

Figure S4. Photovoltaic parameters extracted from current-voltage measurements of the devices with reoptimised concentration of perovskite solution.

Table S1. Photovoltaic parameters extracted from current-voltage measurements of devices with reoptimised pervoskite concentration.

Compact layer (mean ± s.d.)	J_{sc} (mA·cm^{-2})	η (%)	V_{OC} (V)	FF
ht-TiO_2	19.1 ± 1.7	13.0 ± 1.1	1.02 ± 0.04	0.66 ± 0.02
lt-TiO_2	20.9 ± 0.7	14.7 ± 0.9	1.02 ± 0.01	0.69 ± 0.03

3. Characterization of TiO_2 blocking layer films

3.1. Recombination and transport lifetime.

A steady-state background white illumination from an array of diodes (Lumiled Model LXHL-NWE8 whitestar) is first applied to the cell, filling up a fraction of the available sub-bandgap states which will be proportional to the intensity applied. Then, a short pulse was generated from red light diodes (LXHLND98 redstar, 200 ms square pulse width, 100 ns rise and fall time), which is irradiated on the cell and its response is recorded with an oscilloscope. The perturbation light source was set to a suitably low level such that the decay

kinetics were monoexponential. This enabled the charge recombination rate constants to be obtained directly from the exponential decays measured with a 1 GHz Agilent oscilloscope. When the measurement is performed at fixed potential conditions, i.e. potentiostatic mode, the generated charge (DQ) by the pulse can be directly extracted by integrating the photocurrent decay curve. When the measurements is performed at fixed current conditions, i.e. galvanostatic mode, the current generated through the small perturbation pulse is not allowed to exit the device and hence the response measured with oscilloscope is purely dependent on the recombination kinetics of the system, and the perturbation voltage (ΔV) can be extracted. By doing these two measurements at either open or short circuit, we can directly measure the differential capacitance as a function of voltage for the system as C (V) = ΔQ/ΔV.

Recombination lifetime as a function of capacitance (charge density) for the devices employing different compact layers was plotted in a logarithmic scale. Straight lines were fitted to the data points as a guide to the eye.

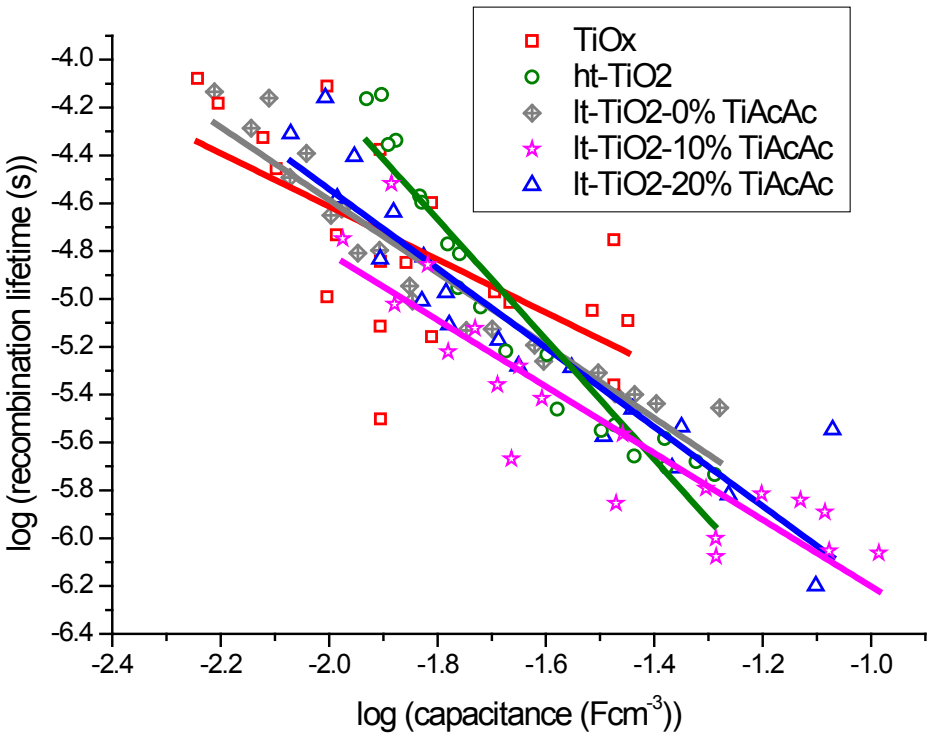

Figure S5. Recombination lifetime at open circuit condition against the differential capacitance.